Tunnelling and Underground Space Technology 70 (2017) 221–232

Contents lists available at ScienceDirect

Tunnelling and Underground Space Technology

journal homepage: www.elsevier.com/locate/tust

2D numerical analysis of rock damage induced by dynamic in-situ stress redistribution and blast loading in underground blasting excavation

J.H. Yang[a], C. Yao[a,*], Q.H. Jiang[a], W.B. Lu[b], S.H. Jiang[a]

[a] School of Civil Engineering and Architecture, Nanchang University, Nanchang 330031, China
[b] State Key Laboratory of Water Resources and Hydropower Engineering Science, Wuhan University, Wuhan 430072, China

ARTICLE INFO

Keywords:
Excavation damage zone
Dynamic in-situ stress redistribution
Blast loading
Peak particle velocity
Numerical simulation

ABSTRACT

When underground cavities are created in initially stressed rock masses by the drill and blast method, an unwanted excavation damage zone (EDZ) is induced around the cavities due to the combined effects of in-situ stress redistribution and blast loading. During rock fragmentation by blasting, the in-situ stress on blast-created excavation boundaries is suddenly released. The in-situ stress redistribution is a dynamic process that starts from the transient release of stress and reaches a final static stress state after excavation. For a circular tunnel that is excavated underground by full-face millisecond delay blasting, 2D finite element simulation is performed to investigate the rock damage induced by the dynamic in-situ stress redistribution and blast loading. The critical peak particle velocity (PPV) for the initiation of blast damage in pre-stressed rock masses is also numerically studied. The results show that the transient stress release generates additional stress waves, resulting in a larger damage zone compared with that following quasi-static stress redistribution. The effect that the additional stress waves have on rock damage becomes more obvious as the in-situ stress levels and excavation dimensions increase and as the stress release duration decreases. Blast-induced tensile stress in the circumferential direction of a tunnel is neutralized by compressive in-situ stress. In deep-buried or high-stressed tunnel excavation, dynamic stress redistribution is responsible for the formation of EDZ; the critical PPV for the initiation of blast damage first increases and then decreases with an increase in the in-situ stress. Therefore, in underground blasting excavation, the factors that affect the level of in-situ stress such as tunnel depths should be considered with respect to the blasting vibration standards and damage criteria.

1. Introduction

In underground mining and civil construction operations involving rock excavation, an undesirable excavation damage zone (EDZ) is created in rock masses surrounding the openings. Excavation-induced rock damage, which can include microcracks, spalling and even v-shaped notches in more severe cases, potentially undermines the tunnel stability and increases the excavation and support costs and delays. Investigating the characteristics and behavior of EDZ is essential for underground openings that require long-term stability. Extensive studies have been conducted to understand and predict the EDZ, and significant advances have been made in determining its formation mechanism and mechanical properties (Martin, 1997; Kaiser et al., 2004; Read, 2004; Martino and Chandler, 2004; Li et al., 2012; Siren et al., 2015; Hao et al., 2016; Lisjak et al., 2016).

The use of explosives is the most cost-effective and widely used rock excavation method. It is generally accepted that when the drill and blast method is used in underground excavation, a combination of the effects of in-situ stress redistribution and blast loading is responsible for the formation of EDZ (Martino and Chandler, 2004). Stress redistribution due to excavation causes local stress concentrations, which may exceed the rock strength, and can damage the rock masses surrounding the excavation. Blast-induced rock damage results from explosion stress waves and subsequent explosion gas expansion.

There are two problems that should be noted in understanding the interaction of in-situ stress redistribution and blast loading. Accompanying rock fragmentation by blasting, the in-situ stress that was initially exerted on the blast-created excavation boundaries is suddenly released. Theoretical and numerical studies have shown that the transient stress release produces stress waves passing through the medium, which cause a transient stress greater than the final static stress (Cook et al., 1966; Carter and Booker, 1990; Li et al., 2014; Zhu et al., 2014). However, many researchers still tend to treat the stress redistribution associated with blasting excavation as a quasi-static process. This approximation is generally acceptable if the in-situ stress level is low. However, at a moderate-to-high stress level, such as

* Corresponding author.
E-mail address: dr.chi.yao@gmail.com (C. Yao).

http://dx.doi.org/10.1016/j.tust.2017.08.007
Received 29 September 2016; Received in revised form 17 July 2017; Accepted 4 August 2017
Available online 08 August 2017

Nomenclature

a	excavation radius
c_f	average crack propagation velocity
c_p	P-wave velocity
D	damage variable
d_b	blasthole diameter
d_c	charge diameter
D_{cr}	damage threshold
E	Young's modulus
F	variable of random distribution
F_0	scale parameter of Weibull distribution
G	shear modulus
$\overline{G}$	degraded shear modulus
K	bulk modulus
$\overline{K}$	degraded bulk modulus
L	charge length
m	shape parameter of Weibull distribution
N	original number of elements
N_f	number of ruptured elements
p_0	in situ stress
P_b	blasting pressure peak on excavation boundaries
$P_b(t)$	blasting pressure-time history on excavation boundaries
P_w	borehole wall pressure
$P_w(t)$	borehole wall pressure-time history
r	distance
R	tunnel radius
S	blasthole spacing
t	time
t_b	initial time of stress release
t_d	stress release duration
t_r	rising time of borehole pressure
V_{cr}	critical peak particle velocity
V_d	velocity of detonation
β	damping factor
γ	specific heat ratio
Δe_{ij}	deviatoric strain increment
δ_{ij}	Kronecker delta
$\Delta\varepsilon_{kk}$	volumetric strain increment
$\Delta\sigma_{ij}$	stress increment
$\dot{\varepsilon}$	strain rate
ε_v	volumetric strain
κ	lateral pressure coefficient
λ	adiabatic expansion constant
ν	Poisson's ratio
ρ	rock density
ρ_e	explosive density
σ_1	maximum principal stress
σ_3	minimum principal stress
σ_c	uniaxial compressive strength
σ_{dc}	dynamic compressive strength
σ_{dt}	dynamic tensile strength
σ_{sc}	static compressive strength
σ_{st}	static tensile strength
σ_t	uniaxial tensile strength
φ	internal frictional angle

20–50 MPa, the strain rate induced by the transient stress release can reach a magnitude of 10^{-1}–10^{1} s^{-1} for most of the short-hole blasts that are used in underground opening excavation (Lu et al., 2012). It is generally acknowledged that when the strain rate exceeds 10^{-1} s^{-1}, the mechanical behavior of rock is a dynamic process and that the inertial effects should not be ignored (Zhang and Zhao, 2014). Therefore, during blasting excavation in highly stressed rock masses, the in-situ stress redistribution around the excavation is a dynamic process that starts from the transient stress release and reaches a final static stress state after excavation. Cai (2008) noted that in addition to blast-induced stress waves and gas pressure, the dynamic unloading or dynamic stress redistribution is another mechanism that may contribute to the formation of EDZ. According to numerical and experimental results, He et al. (2010), Zhu et al. (2014), Yan et al. (2015) and Yang et al. (2015) found that dynamic stress disturbances due to the transient stress release have a considerable influence both on the evolution and extent of EDZ around deep tunnels. Other studies show that the effects of dynamic stress redistribution are closely related to rock properties, in-situ stress levels, stress release rates and paths (Li et al., 2014; Cao et al., 2016; Yang et al., 2016a).

In-situ stress, including its magnitude and orientation, has a significant impact on the distribution and extent of blast-related rock damage zones. Many experimental and numerical studies have shown that when a blasthole is detonated in an initially stressed rock mass, blast-induced cracks are initiated and propagated preferentially along the maximum stress orientation perpendicular to the blasthole axis. The greater the compressive stress is, the more obvious this phenomenon is, and the smaller the cracked zone is (Ma and An, 2008; Omer, 2013; Yilmaz and Unlu, 2013). The pre-loading compressive stress suppresses the blast-induced cracks. High compressive stress may cause fractures around the blasthole, and these fractures may be extended or suppressed by blast-induced stress waves in different patterns (Ma and An, 2008). In addition, the presence of in-situ stress may disturb the propagation of blast-induced stress waves. In this respect, Fan et al. (2009) carried out experimental studies under laboratory conditions. Their results clearly show that the velocity of stress waves increases rapidly with an increase in the in-situ stress at lower levels, but that the velocity tends to be constant under higher stress levels.

Because of these complexities, most studies associated with EDZ tend to investigate individual damage mechanisms separately, such as stress redistribution-induced damage under quasi-static conditions or blast-induced damage for a single blasthole rather than real blasting schemes. It is still unclear how and to what degree the drilling and blasting method affects the formation of EDZ in underground excavation. There are no blasting safety criteria and standards that consider the effects of static in-situ stress and dynamic unloading. Therefore, to fully understand the formation of EDZ in underground blasting excavation, it is significant to numerically study the rock damage induced by the combination of dynamic in-situ stress redistribution and blast loading, with special emphases placed on real blasting schemes and the transient stress release.

In this study, a simplified 2D numerical model is first developed for a circular tunnel excavation using the full-face millisecond delay blasting method. Subsequently, a continuum-based damage model is programmed into the FEM software LS-DYNA to investigate the rock damage evolution induced by dynamic in-situ stress redistribution, blast loading and their combined effects. In addition, the effects of the in-situ stress on the PPV threshold for initiation of blast damage are discussed. These numerical results provide a reference for the blasting safety criteria and standards of underground blasting excavation.

2. Two-dimensional numerical model for blasting excavation of a circular tunnel

Because of the dimensional effect, the behavior of rock damage by a single-hole blast in a stressed rock mass cannot completely represent the picture of rock damage for blasting excavation in underground tunnels. Therefore, to get closer to reality, a model for a circular tunnel excavation is first developed.

2.1. Millisecond delay blasting and its simplified model

It is assumed that a circular tunnel with a radius of 5.0 m is excavated in an infinite geologic body, which is subjected to an in-situ stress field of p_0 (vertical component) and κp_0 (horizontal component). A full-face millisecond delay blasting sequence is employed in the excavation, as shown in Fig. 1. The cutting blastholes in Round I are first detonated, followed by the breaking holes in Round II–IV, buffer holes in Round V and contour holes in Round IV. The delay intervals range from 50 to 150 ms and are controlled by electronic detonators in odd series (MS1, MS3, MS5…). All of the blastholes in the same round are assumed to be detonated at precisely the same time, without considering the delay deviation of detonators. The blast uses blastholes that are 42 mm in diameter and explosives that are 1000 kg/m^3 in density and 3600 m/s in velocity of detonation (VOD). Coupled charge configurations are adopted in the cutting holes, and decoupled charges are used in the other types of blastholes. According to the formal procedures for charge calculations, which are applicable to most tunnel excavation (Persson et al., 1993), the detailed blasthole layout and blasting parameters adopted in this study are listed in Table 1.

A fully 3D model of blasting excavation that incorporates many influence factors obscures the essence of the topic investigated in this study. Therefore, the circular tunnel excavation is simplified to a plane strain problem, and the tunnel is assumed to be located in a homogeneous and isotropic medium. Actual blasting operations in a cycle of tunnel excavation occur over a finite length. In each excavation cycle, the charge columns filled at different depths are not detonated synchronously because of the finite velocity of detonation. Rock discontinuities and the spatial geometry of tunnels also have important effects on the rock damage evolution and distribution. The simplified plane model adopted in this study is limited in these aspects. Despite its limitations, the 2D numerical modeling is still very helpful for clarifying the mechanism of rock damage induced by the combination of dynamic in-situ stress redistribution and blast loading.

When a round of blastholes are detonated simultaneously, the interaction of explosion-induced stress waves from adjacent holes will encourage cracks to spread preferentially along the connecting line of adjacent blastholes (Dare-Bryan et al., 2012). The highly cracked zones between adjacent blastholes become the paths of least resistance for explosion gases to escape and further encourage crack growth in this direction. Accompanying the crack growth and interpenetration throughout the rock between adjacent blastholes, a new free surface, i.e., a blasting excavation boundary, is created along the blasthole line. The normal component of in-situ stress on this boundary is also suddenly released. Therefore, from a macro perspective, the transient release of in-situ stress occurs on the blast-created excavation boundary, i.e., the line that connects blastholes in the same round.

Based on the above, a numerical model that takes the blasting excavation boundary as the inner boundary is developed by using the commercial finite element program ANSYS/LS-DYNA, as shown in Fig. 2. In this way, the full-scale blastholes are not included in this model, and the blasting pressure is applied equivalently to the excavation boundary. This process avoids tremendous model meshing and computational work due to detonations of more than 100 tiny blastholes. The 2D domain measures 100 × 100 m to minimize the boundary effects. After convergence tests, it is discretized into 87,408 quadrilateral elements. In the convergence tests, the size of elements is reduced until the difference of modeling results is less than 5% between consecutive tests. The rock properties of marble in the Jinping-II diversion tunnel project are specified in this study (Li et al., 2012), as listed in Table 2.

2.2. Description of blast loading and transient stress release

The finite element program LS-DYNA has proven to be one of the few codes that allow an accurate description of explosive detonation and explosive-rock interactions. However, such a fine simulation is more suitable for the cases that consist of only a few blastholes. If such a simulation is applied to real tunnel excavation practices, which involve hundreds of blastholes in a blast, as shown in Fig. 1, it will present a considerable challenge for model meshing and computation. Instead, some semi-empirical formulae and detonation theories are used to estimate the explosion pressure. In accordance with the Chapman-Jouguet model of detonation waves, when considering the decoupling effect, the peak pressure exerted on the blasthole wall has the following formula (Fickett and Davis, 1979; Henrych and Major, 1979; Persson et al., 1993):

$$P_w = \frac{\rho_e V d^2}{2(\gamma+1)}\left(\frac{d_c}{d_b}\right)^{2\lambda} \tag{1}$$

where P_w is the borehole wall pressure, ρ_e is the explosive density, V_d is the velocity of detonation, d_c is the charge diameter, d_b is the blasthole diameter, γ is the specific heat ratio, and λ is the explosive's adiabatic expansion constant. For the common explosives used in rock blasting, γ is approximately equal to 3.0 (Persson et al., 1993). The adiabatic expansion constant λ is dependent upon heat of the explosion and detonation velocity, about 1.5 for an average value (Fickett and Davis, 1979; Persson et al., 1993).

The pressure decay function originally proposed by Starfield and Pugliese (1968) and modified by Jong et al. (2005) is adopted to approximate the borehole pressure-time history

$$P_w(t) = 4P_w(e^{-\beta t/\sqrt{2}} - e^{-\sqrt{2}\beta t}) \tag{2}$$

where $P_w(t)$ is the borehole wall pressure-time history, t is time, and β is a damping factor that is determined according to the rising time of borehole pressure to its peak. From Eq. (2), the peak pressure occurs at time $t_r = -\sqrt{2}\ln(1/2)/\beta$; hence, the damping factor β is expressed as

$$\beta = -\sqrt{2}\ln(1/2)/t_r \tag{3}$$

At present, there is some controversy with respect to the peak pressure attainment time. Many publications cite the rising time of borehole pressure in the order of several microseconds, but some of the literature suggests that it is in the order of hundreds of microseconds to several milliseconds. For a cylindrical charge column, Lu et al. (2012) deemed that after the detonation waves are propagated through the column of explosive, the borehole pressure rises to a maximum. Thus,

$$t_r = L/V_d \tag{4}$$

where L is the charge length.

An important simplification in this numerical study is to transfer the borehole pressure equivalently onto the blasting excavation boundary to solve the problem of multi-hole blasts. According to the

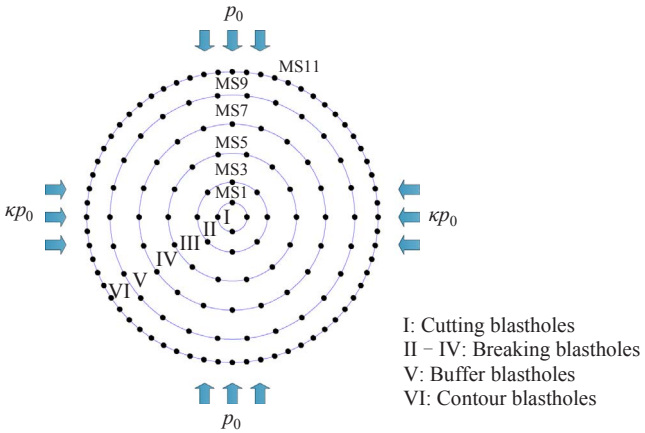

Fig. 1. An underground tunnel excavation with the method of full-face millisecond delay blasting.

Table 1
Drilling and blasting parameters for the full-face millisecond delay blasting.

Blasthole type	Cutting holes	Breaking holes			Buffer holes	Contour holes
Initiation sequence	I	II	III	IV	V	VI
Detonator series	MS1	MS3	MS5	MS7	MS9	MS11
Delay time (ms)	0	50	110	200	310	460
Blasthole diameter (mm)	42.0	42.0	42.0	42.0	42.0	42.0
Charge diameter (mm)	42.0	32.0	32.0	32.0	28.5[a]	25.0
Spacing (m)	0.7	0.8	1.0	1.0	1.0	0.5
Distance to the tunnel center (m)	0.5	1.2	2.2	3.2	4.2	5.0

[a] The buffer blastholes are filled with the half-and-half mixing charge of 32 mm and 25 mm in diameters, and thus a mean diameter is adopted in the table.

Saint–Venant's principle, the equivalent blasting pressure on the excavation boundary is determined by

$$P_b(t) = (d_b/S)P_w(t) \tag{5}$$

where $P_b(t)$ is the blasting pressure-time history on the excavation boundary and S is the spacing between adjacent blastholes in the same round.

This equivalent treatment causes some deviation in the immediate vicinity of blastholes. However, this study is to investigate the rock damage outside the tunnel profile rather than the explosion-induced rock fracture and fragmentation process around blastholes. Therefore, this equivalent processing is acceptable to a certain degree (Torano et al., 2006; Xia et al., 2013). From Eqs. (1)–(5), the blasting pressure-time profile on the excavation boundary is shown in Fig. 2; the time of pressure rise to its peak and the duration are approximately 0.8 and 8.0 ms.

Three parameters must be specified to describe the transient release of in-situ stress on excavation boundaries: the magnitude of the initial stress, the stress release duration and the release path. As mentioned earlier, the transient stress release occurs with the blast-induced cracking throughout the connecting line of adjacent blastholes in the same round. Therefore, when the cracks are considered to be propagated at a constant velocity, the stress release duration can be approximated by

$$t_d = \frac{\sqrt{\left(\frac{1}{2}S\right)^2 + L^2}}{c_f} \tag{6}$$

Table 2
Rock properties in the finite element calculations.

Properties	Value
Density, ρ (kg/m^3)	2700
Young's modulus, E (GPa)	50
Poisson's ratio, ν	0.22
Uniaxial compressive strength, σ_c (MPa)	80
Uniaxial tensile strength, σ_t (MPa)	5
Internal frictional angle, φ (°)	38

where t_d is the duration of the transient stress release and c_f is the average velocity of crack propagation. According to the Griffith's rupture criterion, the average cracking velocity is 20–30% of the velocity at which P-waves are propagated through the medium.

In cylindrical charges, the explosion-induced stress wave radiation and rock cracking in the near field is dominated completely by P-Mach and S-Mach waves because of the detonation wave propagation (Blair, 2014). Therefore, in spite of the 2D numerical analyses, the effect of charge length on the crack propagation duration is still considered to come closer to reality. Substituting the related blasting parameters and rock properties into Eq. (6) yields a duration of 2.6 ms for the transient stress release in all rounds. In a rock mass characterized by a P-wave velocity of 4000–6000 m/s and S-wave velocity of 2000–3000 m/s, the stress waves generated by transient stress release at the excavation boundaries travel through the burden of 0.5–1.0 m (see Table 1) within 0.5 ms. The delay intervals of blasts between adjacent rounds are at least 50 ms. Thus, before the current round of blastholes is detonated, the transient unloading stress waves from the former round have passed over the blasting excavation boundary of the current round. Therefore, for the millisecond delay blasting in Fig. 1, the initial stress on the excavation boundaries to be released is a redistributed secondary stress after the blasts of the former delay.

Rock fragmentation by blasting is a very fast and complicated process, and it is very difficult to clarify the path for the transient stress release that occurs in this process. Most researchers tend to address it by using linear, cosinoidal and exponential functions (Carter and Booker, 1990; Zhu et al., 2014; Li et al., 2014). In this study, a linear path in which the initial stress is released at a constant rate over the duration is adopted, as shown in Fig. 2. According to the stress continuity condition, when the blasting pressure falls to a level equal to the initial stress on excavation boundaries, the in-situ stress release begins to occur at time $t = t_b$.

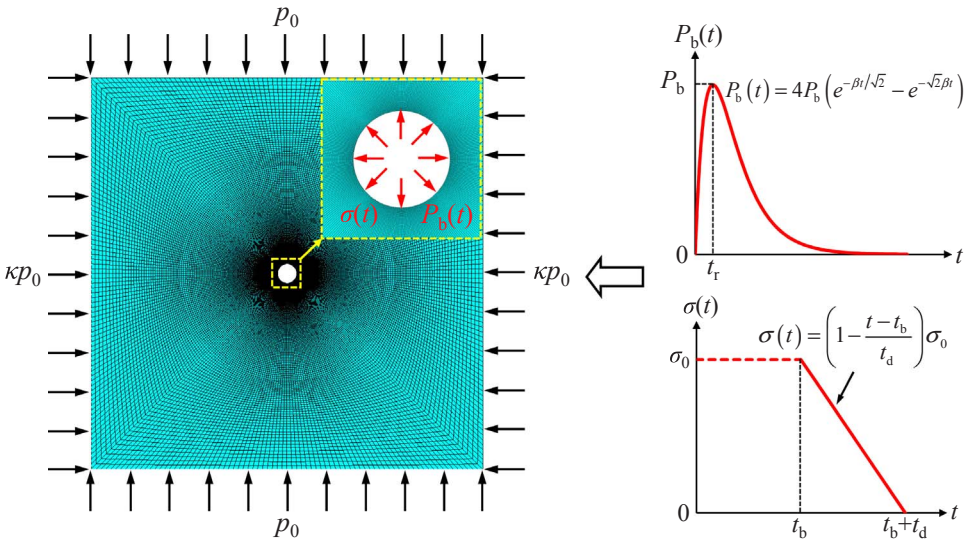

Fig. 2. The finite element model and loads used for the numerical calculations.

2.3. Rock damage model

Based on the physical nature of brittle damage phenomena, Krajcinovic and Silva (1982) proposed a simple but efficient damage law. In this damage model, rock materials are assumed to be composed of a series of tiny elements. Each element remains completely elastic until it ruptures when the force reaches its rupture strength. The actual damage law is a distribution function of the rupture strength of individual elements. Assuming that the strength follows the Weibull distribution, at a force of F, the number of already ruptured elements is

$$N_f = N\left\{1-\exp\left[-\left(\frac{F}{F_0}\right)^m\right]\right\} \tag{7}$$

where N_f is the number of ruptured elements, N is the original number of elements, and F_0 and m are scale and shape parameters of the Weibull distribution. According to Krajcinovic and Silva (1982), the scale parameter F_0 represents the average strength of macroscopic rock, and the shape parameter m identifies the concentration degree of rock element strength distribution.

Damage development in the macroscopic rock is regarded as a continuous process of rock element rupture. Thus, the non-negative damage variable D is defined as a ratio of the number of already ruptured elements to the original number of elements. Then,

$$D = \frac{N_f}{N} = 1-\exp\left[-\left(\frac{F}{F_0}\right)^m\right] \tag{8}$$

Many experimental and numerical studies show that rock subjected to explosion pressure or stress redistribution is fractured in tension or compression-shear mode (Kaiser et al., 2004; Zhu et al., 2007; Ma and An, 2008; Zhang et al., 2010; Yilmaz and Unlu, 2013; Wei et al., 2017; Yao et al., 2017). In this study, the maximum tensile stress criterion and the Mohr-Coulomb criterion are, respectively, used as the rock strength criterion in tension and shear. Under the convention of compression positive, the variable F regarding the stress state can be expressed as

$$F_t = f(\sigma) = -\sigma_3 \tag{9}$$

$$F_c = f(\sigma) = \sigma_1 - \frac{1+\sin\varphi}{1-\sin\varphi}\sigma_3 \tag{10}$$

The damage variable D in tension or compression-shear mode can be calculated as

$$D_t = 1-\exp\left[-\left(\frac{F_t}{F_t}\right)^{m_t}\right] \quad \varepsilon_V \leqslant 0 \tag{11}$$

$$D_c = 1-\exp\left[-\left(\frac{F_c}{F_{0c}}\right)^{m_c}\right] \quad \varepsilon_V > 0 \tag{12}$$

where σ_1 and σ_3 are the maximum and minimum principal stress, σ_t and σ_c are the tensile strength and compressive strength of rock, φ is the internal frictional angle, ε_v is the volumetric strain, and the subscripts t and c represent the tension mode and compression-shear mode.

In an elastic and continuum-based damage model, rock damage evolution is described as a process of Young's modulus degradation. According to the elastic relationship between Young's modulus and acoustic velocity in rock materials, the damage variable threshold D_{cr} at which considerable damage begins to occur is 0.20 (Li et al., 2011). Under dynamic loading or unloading conditions, rock strength is strain-rate-dependent. According to the study of Li and Gu (1994), the dynamic compressive and tensile strength can be estimated by

$$\sigma_{dc} = \sigma_{sc}\dot{\varepsilon}^{1/3} \tag{13}$$

$$\sigma_{dt} = \sigma_{st}\dot{\varepsilon}^{1/3} \tag{14}$$

where σ_{dc} and σ_{dt} are the dynamic compressive and tensile strength of rock, σ_{sc} and σ_{st} are the static compressive and tensile strength, and $\dot{\varepsilon}$ is the strain rate. Since the scale parameter F_0 in Eq. (7) represents the average strength of macroscopic rock, it is considered that $F_{0t} = \sigma_{dt}$ and $F_{0c} = \sigma_{dc}$.

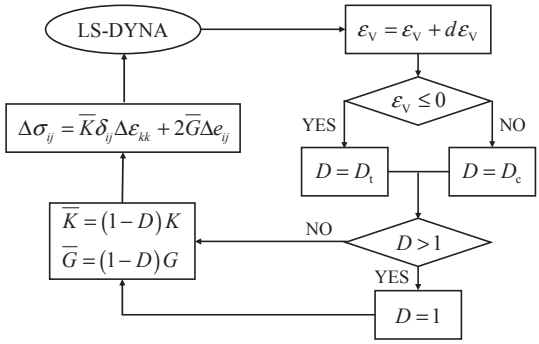

Fig. 3. Flowchart for the numerical implementation of the rock damage model.

From Eqs. (1)–(5), the maximum blasting pressure peak applied to the excavation boundaries is 97.2 MPa, which occurs in the blast of cutting holes. The rising time to its peak is approximately 0.8 ms. Given a Young's modulus of 50 GPa, under the one-dimensional and elastic conditions, it can be estimated from $\dot{\varepsilon} = P_{b0}/(Et_r)$ that the maximum strain rate induced by the equivalent blast loading is in the magnitude of $10^1\ s^{-1}$.

2.4. Numerical verification and simulation scheme

In this study, the above rock damage model is embedded into the FEM program LS-DYNA through its user subroutines. The numerical implementation algorithm is developed as shown in Fig. 3. Because the tensile strength of rock is much lower than its compressive strength, rock materials are more readily damaged in tension mode. Therefore, in the numerical implementation of Eqs. (11) and (12), the formula $\varepsilon_V \leqslant 0$ is first used to check whether the tensile damage occurs in rock elements. It is assumed that the rock density and Poisson's ratio are unchanged as the damage develops. According to the principle of elastic damage, the degraded bulk modulus $\overline{K} = (1-D)K$ and shear modulus $\overline{G} = (1-D)G$ are considered for the damaged rock elements, where K and G are the initial bulk modulus and shear modulus.

A comparison of rock damage between numerical modeling and site survey is made to validate the developed rock damage model. The site test is a single vertical hole blast carried out by Li et al. (2011) in the bedrock blasting excavation of the Linao Nuclear Power Plant Project (LNPP). By using their blasting parameters and rock properties, the blast-induced damage simulated from the above damage model is shown in Fig. 4. At the damage threshold $D_{cr} = 0.20$, the maximum damage radius is 6.5 m, and the damage depth at the hole bottom is 2.1 m. Acoustic detection shows that the damage radius and depth are 6.6 m and 2.3 m. A good agreement with the experimental data indicates that this damage model is feasible for predicting blast-induced rock damage. A similar verification has also been conducted by Xie et al. (2016) and demonstrates its validity.

During underground blasting excavation, the rock surrounding the opening is subjected to pre-existing in-situ stress followed by excavation disturbances, including dynamic stress redistribution and blast loading. Implementation of this numerical modeling involves two steps, static stress initialization and dynamic loading or unloading. This systematic process can be performed in the commercial FEM software ANSYS/LS-DYNA by using its implicit solution and explicit solution in sequence, as shown in Fig. 5. The restart analysis in the LS-DYNA program is utilized to reproduce the millisecond delay blasting sequence. The rock stress and deformation calculated from the current delay are submitted to the calculations of the next delay as the initial conditions to maintain succession. The computing time for each delay is set as the interval time of detonators (see Table 1).

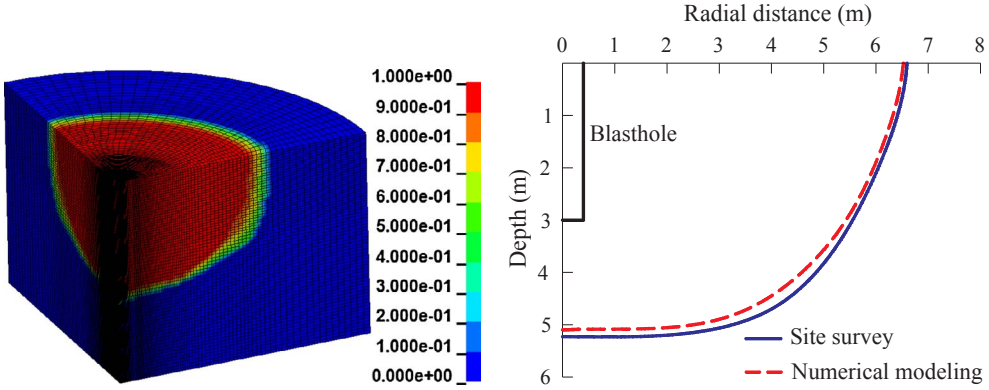

Fig. 4. Comparison of blast-induced rock damage of numerical modeling and site survey.

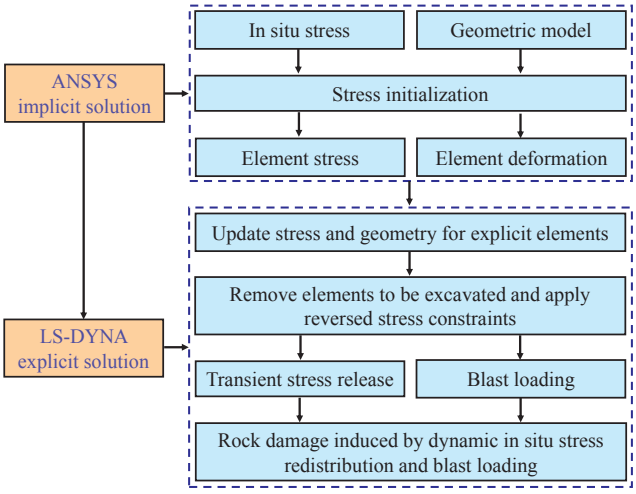

Fig. 5. Procedure of the implicit and explicit solution in sequence in ANSYS/LS-DYNA.

The rock damage modeling is based on a continuum damage model, and a pressure-decay function is directly input into the code to approximate the blasting pressure. Thus, the numerical modeling presented in this paper is concerned only with the blast damage caused by stress waves, without considering the detonation gas flow and gas-driven crack propagation.

3. Rock damage induced by dynamic in-situ stress redistribution

Fig. 6 presents the radial, circumferential and deviatoric stress histories at the distance $r = 2a$ (a is the excavation radius and equals 5.0 m) for a stress release duration of $t_d = 2.6$ ms. As seen from this illustration, when the stress release disturbance reaches the observation point, the radial stress first decreases substantially, then rebounds and finally stabilizes in a static stress state (secondary stress). The circumferential stress first increases rapidly, then decreases and finally remains stable. The maximum magnitude of the dynamic circumferential stress at $r = 2a$ is 9.0% greater than the final static value, and the minimum magnitude of the dynamic radial stress is smaller by 34.1% than the final secondary stress. The additional dynamic stress due to the transient stress release will become more substantial for a shorter release duration.

In deep tunnel excavation, it is generally acknowledged that rock damage begins as a result of the removal of radial confining stress and the loading by circumferential stress concentration. In the immediate vicinity of the excavation boundary, the confining stress is low, varying between 0 and a few MPa. In such a stress state, microcracks tend to grow in the direction parallel to the maximum compressive stress and then create a spalling of rock parallel to the tunnel wall (Martin, 1997). Many experiments indicate that, in uniaxial or unconfined compression, two different modes of fracture may occur: (a) local 'tensile' fracture predominantly parallel to the applied stress, and (b) macroscopic shear fracture (faulting). However, with an increase in the confining stress, the tensile fracture is suppressed, and the shear fracture develops in the interiors and gradually becomes the main failure mechanism (Zhang et al., 2010). In uniaxial compression, the crack initiation for most rocks occurs at an applied stress of 0.3–0.5σ_c. For confined rocks, the crack initiation threshold is generally described by a constant-deviatoric stress limit (Cai et al., 2004). Since the dynamic stress redistribution causes higher circumferential and deviatoric stress than the final static value, as shown in Fig. 6, it may cause more severe rock damage.

For the full-face millisecond delay blasting in which the rock mass to be excavated is removed layer by layer (see Fig. 1), this section first presents the evolution process of rock damage caused by dynamic in-situ stress redistribution. The dynamic effects of the transient stress release on rock damage and its influence factors are subsequently investigated.

3.1. Rock damage evolution process

Fig. 7 shows the evolution process of rock damage due to dynamic stress redistribution when the vertical in-situ stress p_0 is equal to 30 MPa and the lateral pressure coefficient κ is 1.0. In each blast delay, a thin excavation damage zone is induced in the close vicinity of the excavation boundaries by the dynamic stress redistribution. As the excavation boundaries in the first four delays are far from the tunnel profile, the damage zone does not extend into the tunnel wall until blasts of the fifth delay (MS9 delay). After detonation of the last delay (MS11 delay), the damage finally extends to a depth of 1.20 m into the rock mass outside the tunnel profile.

If the stress release occurring on excavation boundaries is treated as a quasi-static process, the rock damage is completely attributed to the

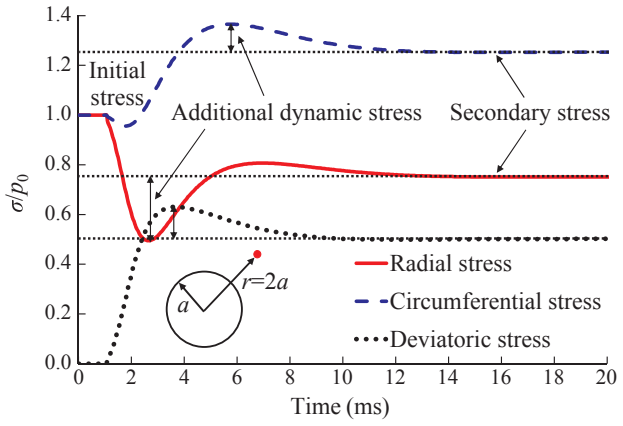

Fig. 6. Stress-time histories of the dynamic in-situ stress redistribution.

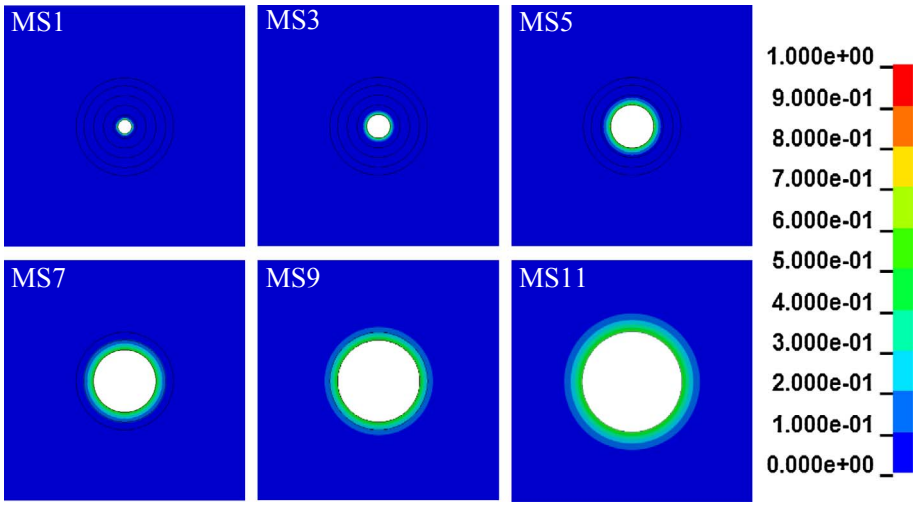

Fig. 7. Rock damage evolution caused by dynamic in-situ stress redistribution during the full-face millisecond delay blasting (p_0 = 30 MPa and κ = 1.0).

final static stress (secondary stress). In this case, the final damage depth is 0.98 m, as shown in Fig. 8. Compared with the quasi-static stress redistribution, the additional dynamic stress due to transient stress release causes an increase of 22.4% in damage depth. Fig. 8 also presents the final EDZ distribution at the lateral pressure coefficient κ = 2.0. The damage zone is mainly found in the roof and floor because of high compressive stress concentration in this region. This means that compression-shear failure is the major mechanism for the rock damage caused by dynamic in-situ stress redistribution. Cook et al. (1966) and Zhu et al. (2014) found that when the duration of stress release is sufficiently short, e.g., less than 0.2 ms, dynamic tensile stress can be generated, and a very shallow tensile damage zone is created in the sidewall. In the present study, no tensile damage zone is found around the opening because a much longer stress release duration of 2.6 ms is adopted for the blasthole layout. At the lateral pressure coefficient κ = 2.0, the final damage depth is increased by 26.5% due to the additional dynamic stress.

3.2. Analysis of influence factors

According to the analytical solution to the problem of sudden excavation of a circular tunnel in an elastic ground (Carter and Booker, 1990; Zhu et al., 2014), the factors that affect the dynamic stress redistribution include but are not limited to the magnitude of the in-situ stress, the duration of stress release, the dimension of the excavation boundaries and the rock properties. For the given rock properties listed in Table 2, this study evaluates the effects of the other three factors on rock damage. Fig. 9 shows the final damage zones under different far-field stress magnitudes, stress release durations and excavation dimensions when the lateral pressure coefficient κ is 1.0. Under far-field stresses of p_0 = 30, 40 and 50 MPa, the damage depth into the tunnel profile induced by dynamic stress redistribution is approximately 1.20, 2.74 and 5.86 m, respectively, which are 22.4%, 28.3% and 31.3% greater than the damage zone induced by quasi-static stress redistribution. At p_0 = 30 MPa and an excavation radius a = 5.0 m, the damage depth induced by dynamic stress redistribution is increased by 22.4%, 14.3% and 7.1%, respectively, for stress release durations of t_d = 2.6, 5.2 and 10.4 ms. When the far-field stress and the stress release duration are constant (p_0 = 30 MPa and t_d = 2.6 ms), the damage zone extends 0.29, 0.52 and 1.20 m into the tunnel wall for a = 1.2, 2.2 and 5.0 m, respectively, for an increase of 19.7%, 21.9% and 22.4% over the quasi-static condition.

From a comparison of the absolute damage depth, the dynamic stress redistribution-induced damage will grow to a larger zone as the in-situ stress magnitude and excavation dimension increase. For the percentage of increase in damage depth, with increases in the stress level and excavation dimension, the additional dynamic stress due to transient stress release will become more obvious and, accordingly, contribute more to the formation of EDZ. The additional dynamic stress and resultant damage will increase as the duration of stress release decreases. No matter how these influence factors change, the rate of damage increase resulting from the additional dynamic stress is no more than 100%. The static component of dynamic stress redistribution (equal to the secondary stress) dominates the rock damage, and the additional dynamic stress waves cause further growth and degradation to the damage zone. Therefore, the transient stress release and induced stress waves are very important subjects in the evaluation of EDZ, especially for large-scale blasting excavations in highly stressed rock masses.

4. Rock damage induced by the combination of dynamic stress redistribution and blast loading

4.1. Rock damage under repeated blast loading

When the far-field in-situ stress p_0 is equal to 0 MPa, development of the rock damage induced by the repeated blast loading is shown in Fig. 10. Although a fully coupled charge is used, blasts of the cutting holes in the MS1 delay do not cause damage to the rock outside the

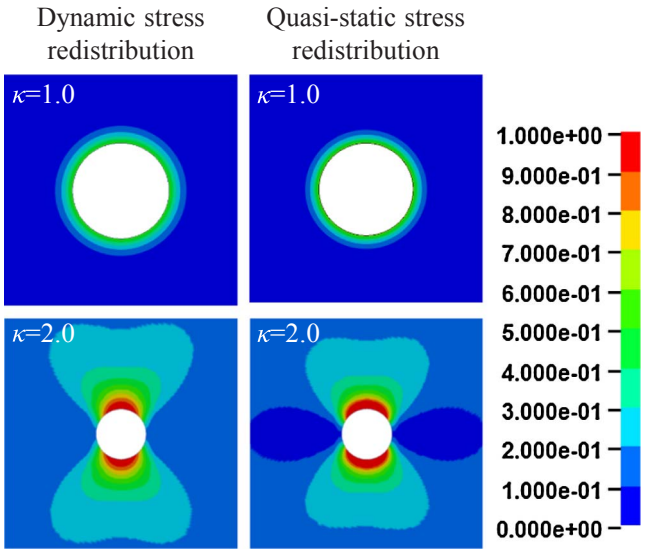

Fig. 8. Comparison of the final damage extent of dynamic stress redistribution and quasi-static stress redistribution (p_0 = 30 MPa).

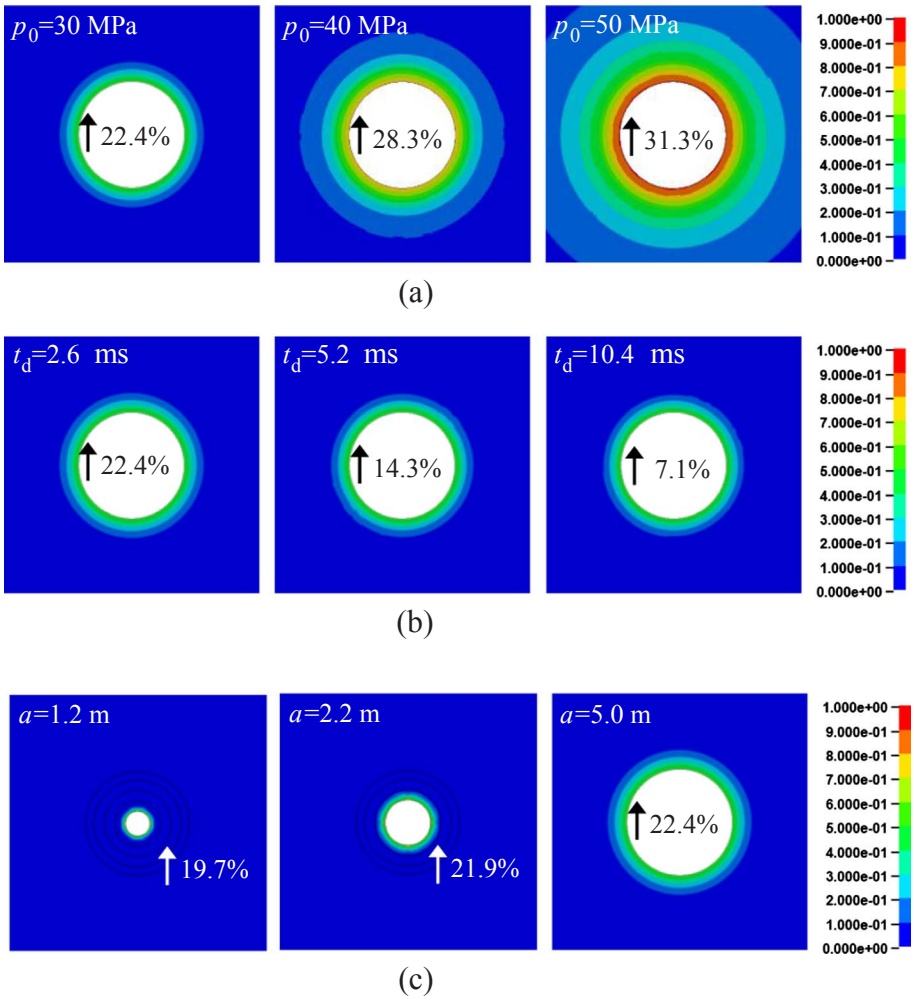

Fig. 9. Dynamic stress redistribution-induced rock damage zones under different boundary conditions (κ = 1.0): (a) under different magnitudes of far-field in-situ stress; (b) under different durations of in-situ stress release and (c) under different excavation dimensions.

tunnel perimeter because of a far distance. As the blastholes in outer rows detonate, the blast-induced rock damage extends into the tunnel profile and spreads rapidly. After blasts of the first row of breaking holes (MS3 delay), the damage depth into the tunnel profile is only 0.57 m. However, it is increased substantially to 4.46 m after completing the third row of breaking holes (MS7 delay). The rock damage beyond the tunnel profile finally persists to a depth of 6.39 m after the final row of blastholes are blasted. The use of decoupling explosives significantly reduces the pressure on the buffer and contour hole walls, and the damage growth from the last two delays is relatively smaller. Blasts of the outermost breaking holes contribute the most to the formation of the final damage zone. Therefore, sufficient attention should be paid to the charge design of the breaking holes in addition to the final contour row.

Cautious blasting methods use peak particle velocity (PPV) to predict the damage zone associated with a particular explosive charge for a given rock mass (Holmberg and Persson, 1980). The intersection of the PPV attenuation curve with the damage distance yields the PPV

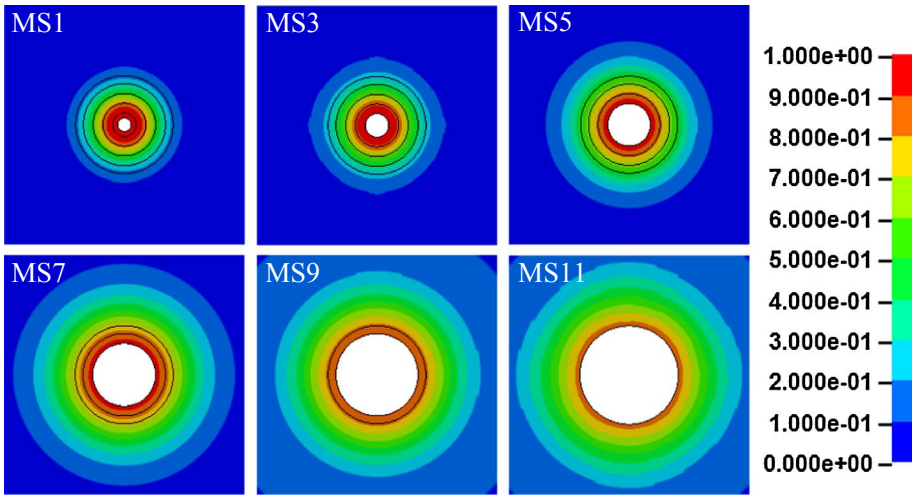

Fig. 10. Rock damage evolution induced by blast loading during the full-face millisecond delay blasting (p_0 = 0).

threshold or limit for initiation of blast-induced damage. The repeated blast loading in the millisecond delay blasting sequence causes damage accumulation and generally results in a relatively excessive damage depth than does a single blast loading. Repeated blasts at low levels can eventually create damage equivalent to a single event at a high level. Therefore, for millisecond delay blasting, the damage accumulation should be considered when determining the PPV threshold. From our numerical results, the accumulated damage extends to a depth of 6.39 m into the tunnel profile, where the PPV threshold is 50.2 cm/s in the MS11 delay, as shown in Fig. 11. If the accumulated damage from the previous delays is not considered, the single blast loading in the MS11 delay creates a damage depth of 5.86 m. At this distance, the PPV is 59.5 cm/s. The repeated blast loading in this model results in a 15.6% reduction in the PPV threshold for the initiation of blast-induced damage.

The above result is based on a millisecond delay blasting sequence in only one excavation cycle, and the number of repeated blast loadings is only six. In fact, the rock surrounding the tunnel profile is subjected to many occurrences of blast loading with advancement of the blasting work face. In this situation, the PPV threshold will decrease. For instance, the field tests conducted by Ramulu et al. (2009) show that after 45–50 occurrences of blast loading, the PPV threshold is reduced to approximately 20% of the initial value in basalt. This finding is similar to the observations of Adamson and Scherpenisse (1998). Stagg et al. (1984) stated that in repeated blast loading conditions, the vibration level at 50% of the value in one fold can cause rock damage.

4.2. Rock damage under dynamic stress redistribution and blast loading

In underground blasting excavation, damage is induced in the rock surrounding the excavation by a combination of the effects of stress redistribution and blast loading. In the numerical simulation, the far-field in-situ stress is varied from 0 to 30 MPa (i.e., 0, 5, 10, 20 and 30 MPa) to investigate the damage zone distribution induced by the combined actions of dynamic stress redistribution and blast loading. After modeling the millisecond delay blasting process from MS1 to MS11 delay, Fig. 12(a) shows the final damage zone distribution after excavation at the lateral pressure coefficient $\kappa = 1.0$. It is clear that at lower in-situ stress levels (e.g., 0, 5 and 10 MPa), dynamic stress redistribution does not create rock damage at all, and the development of EDZ is primarily attributed to repeated blast loading. Many researchers tend to subdivide the blast-induced damage zone around a blasthole into a crushed zone and a cracked zone. Theoretical and numerical studies have indicated that the shear stress resulting from the high radial borehole pressure causes a thin crushed zone in the immediate vicinity of the blasthole wall and that circumferential tensile stress creates radial cracks, which spread longer and form a wider cracked zone (Zhu et al., 2007; Ma and An, 2008; Yilmaz and Unlu, 2013; Li et al., 2017). For this reason, the crushed zone can be considered as a compression-shear damage zone, and the cracked zone can be considered as a tensile damage zone. Generally, the width of the compression-shear damage zone is much smaller than that of the tensile damage zone because the tensile strength of rock is much lower than its compressive strength. The radial fracture caused by the circumferential tensile stress is the main mechanism of blast-induced damage, especially in the region farther from the blast-hole walls.

Because the breaking blastholes are far away from the tunnel wall, no blast-induced compression-shear damage, only tensile damage, is found in the rock beyond the tunnel profile. At lower in-situ stress levels (0, 5 and 10 MPa), the extent of the tensile damage zone caused by blast-induced circumferential stress narrows quickly with the increase of the in-situ stress level, as shown in Fig. 12(a). It is because the blast-induced circumferential tensile stress is neutralized by the compressive in-situ stress. The dynamic stress redistribution causes circumferential compression stress concentration around the tunnel wall, and the blast-induced tensile damage is impressionable to the existence of in-situ stress. When the far-field stress reaches a higher level, e.g., 20 MPa, because the dynamic stress redistribution-related compression-shear damage is initiated, the damage zone outside the tunnel contour expands as the magnitude of in-situ stress increases.

Fig. 12(b) shows the final distribution of rock damage induced by the combination of dynamic stress redistribution and blast loading at the lateral pressure coefficient $\kappa = 2.0$. As the in-situ stress level increases, the damaged zones are distributed in different patterns. At lower in-situ stress levels, such as $p_0 = 5.0$ MPa, because the blast-induced circumferential tension stress is neutralized in the roof and floor by the concentrated compressive in-situ stress, the rock damage is only found in the sidewall. At $p_0 = 20.0$ MPa or higher, the rock damage caused by the dynamic stress redistribution is aligned along the minimum stress orientation and located in the roof and floor. From Fig. 12 and the above discussion, it can be concluded that during blasting excavation in highly stressed rock masses, blast-induced rock damage is limited in a very small zone near the blasthole walls, and dynamic in-situ stress redistribution is the main mechanism for the development of EDZ surrounding the tunnel profile.

At $p_0 = 30$ MPa and $\kappa = 1.0$, the final damage induced by the combined actions of dynamic stress redistribution and blast loading extends to a depth of 1.32 m into the tunnel profile. If the in-situ stress release occurring on blast-created excavation boundaries is treated as a quasi-static process, the damage depth is 1.10 m for the combination of static secondary stress and blast loading, as shown in Fig. 13. As calculated in Section 3.1, the individual effect of the static secondary stress results in a damage depth of 0.98 m into the tunnel wall. The blast-induced stress waves lead to an increase of 12% in the damage depth (1.10 m vs 0.98 m), whereas the increase due to the additional dynamic stress caused by transient stress release is 20% (1.32 m vs 1.10 m). It follows that under high in-situ stress conditions, the transient unloading-produced additional stress waves contribute more to the rock damage than do the blasting stress waves. The damage due to the final static secondary stress (0.98 m) accounts for approximately 74% of the total damage depth (1.32 m), and thus, the static component of stress redistribution is mainly responsible for the formation of EDZ. Although the contribution to the total damage depth is smaller, the stress waves resulting from both transient unloading and blast loading often play a role in triggering damage initiation to the rock mass in a critical damage state under the static in-situ stress.

4.3. Discussion of the practical consequences of the numerical results

The peak particle velocity is widely used as a principal evaluation index in current blasting vibration standards and damage criteria. As mentioned earlier, the PPV threshold for initiating blast-induced damage is the velocity value at the damage distance. Because the blast

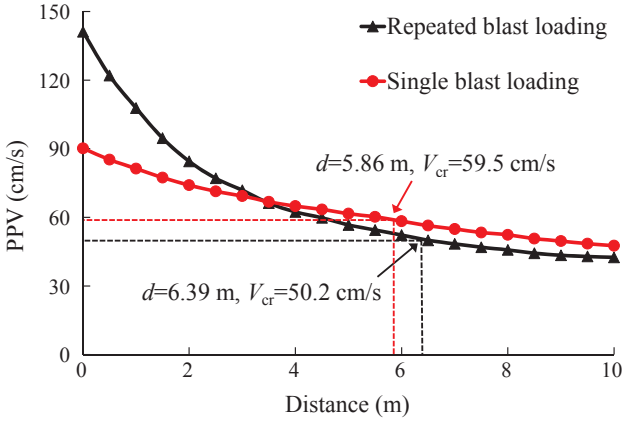

Fig. 11. Determination of the PPV threshold for initiation of blast-induced damage (MS11 delay).

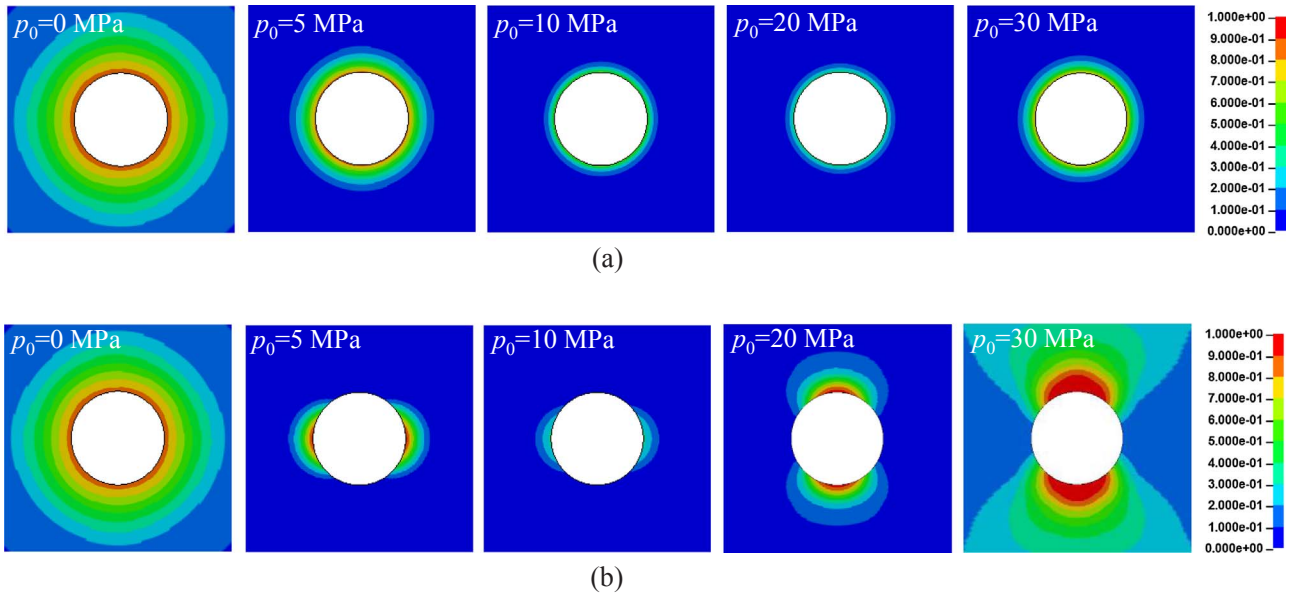

Fig. 12. Final damage zones induced by the combined action of dynamic stress redistribution and blast loading under different in-situ stress levels: (a) $\kappa = 1.0$ and (b) $\kappa = 2.0$.

damage distribution is easily affected by the pre-existing in-situ stress (see Fig. 12), the PPV threshold for blast damage initiation in deep tunnels must be different from that in shallow tunnels.

Taking blasts of the outermost breaking holes in the MS7 delay as an example, at different in-situ stress levels varying between 0 and 30 MPa, the PPV attenuation curves with damage distances are shown in Fig. 14. At stress levels of 0, 5 and 10 MPa, the PPV threshold for initiating blast damage is 52.3, 61.9 and 69.0 cm/s. Because blast-produced circumferential tensile stress and resultant tensile damage are suppressed by the compressive in-situ stress, the PPV threshold is increased as the in-situ stress level increases within a certain range. Compared to the shallow tunnels, the maximum allowable charge weight per delay for the tunnels at moderate depth can be increased accordingly. However, when the in-situ stress is sufficiently high to cause rock damage due to dynamic stress redistribution, in the already damaged rock mass, the PPV threshold for blast damage initiation will decline. A less charge is required to prevent rock damage growth and aggravation from blasting. As shown in Fig. 14, at $p_0 = 30$ MPa, the PPV threshold is 12.7% smaller than that observed at $p_0 = 20$ MPa.

The PPV threshold and the maximum allowable charge for initiation of blast damage first increase and then decrease with the increase of in-situ stress, as shown in Fig. 14. Therefore, in underground blasting excavation, the effects of in-situ stress should be considered in the blasting vibration standards and damage criteria. Different PPV thresholds are required according to the tunnel depths and in-situ stress levels. This also indicates that in underground blasting excavation, it is not appropriate to estimate the blast PPV threshold by using only the tensile strength of rock without considering the in-situ stress state.

In deep tunnels under high in-situ stress conditions, the dynamic stress redistribution is responsible for the formation of rock damage. To minimize the stress redistribution-induced damage, the additional dynamic stress from the transient stress release should be reduced by properly designing excavation procedures and blasting geometry. For those tunnels with a large cross-section, it is advisable to use upper and lower bench blasting methods instead of full-face blasting methods to reduce the excavation dimension in a blast. The use of a smaller burden reduces the stress on blast-created excavation boundaries, and larger blasthole spacing extends the duration of transient stress release. According to the numerical analyses in Section 3.2, these measures all contribute to reducing the effects of the additional dynamic stress. An appropriate blasthole detonation sequence can also considerably reduce the dynamic disturbance of transient stress release. For example, the blastholes located in the region of lower stress are first detonated followed by those in the vicinity of the stress concentration zones. In this way, part of the strain energy stored in the stress concentration zones can release early due to blast-created free surfaces. It mitigates the subsequent strain energy release when the concentrated stress zones are blasted (Yang et al., 2016b). All of these measures should be carried out in an attempt to ensure satisfactory rock fragmentation.

5. Conclusions

During underground blasting excavation, the in-situ stress redistribution is a dynamic process that starts from the transient release of stress on excavation boundaries and reaches the final static secondary stress after excavation. The transient stress release generates additional stress fluctuations prior to the final static stress. In this study, 2D numerical simulation is conducted to investigate the rock damage induced by the dynamic stress redistribution and blast loading. Compared to the quasi-static process, the dynamic stress redistribution creates a larger rock damage zone due to the additional stress fluctuations. The contribution of the additional stress waves to rock damage becomes more

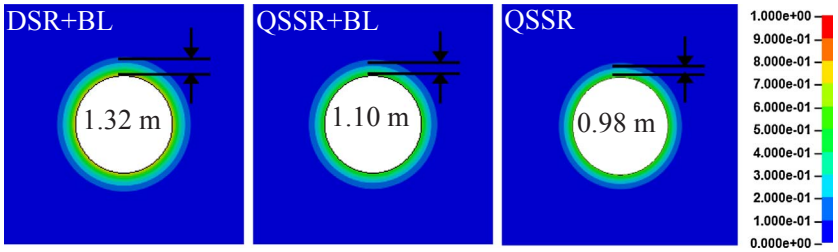

Fig. 13. Final damage zones under different loading combinations (DSR, QSSR and BL represent dynamic stress redistribution, quasi-static stress redistribution and blast loading, respectively).

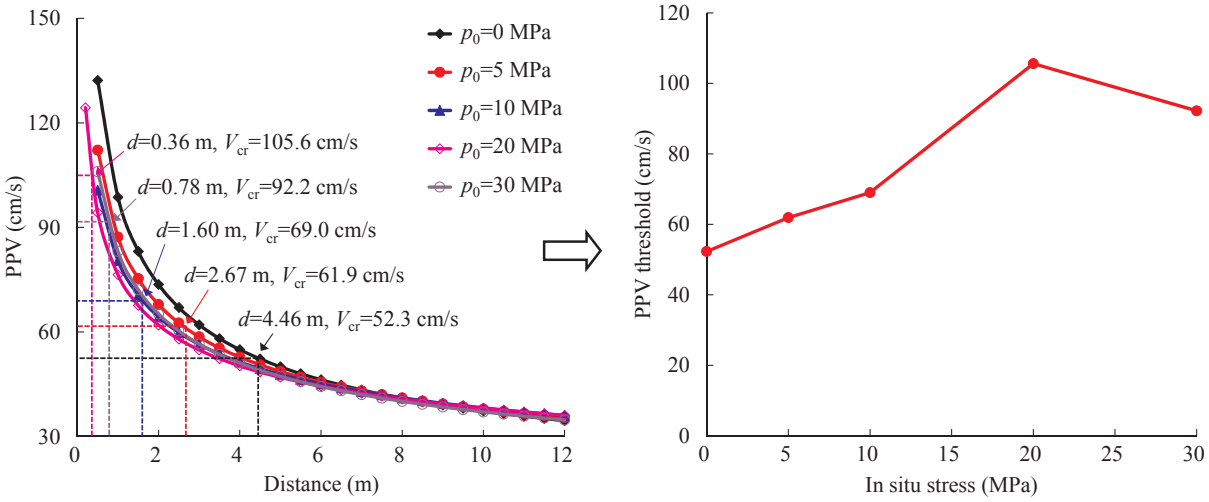

Fig. 14. PPV thresholds for initiation of blast-induced damage under different in-situ stress levels (MS7 delay).

obvious as the in-situ stress levels and excavation dimensions increase and as the stress release duration decreases. Therefore, in the assessment of EDZ, extra care should be taken to consider the additional stress waves arising from the transient stress release occurring on blast-created excavation boundaries, especially for large-scale blasting excavations in highly stressed rock masses. To minimize the rock damage extension and aggravation from the additional stress waves, it is recommended to use upper and lower bench blasting methods, smaller burdens and larger spacing for deep tunnel blasting excavation.

Tensile fracture caused by circumferential tensile stress is the main mechanism for blast-induced rock damage around the tunnel profile. In underground blasts, the blast-produced circumferential tensile stress beyond the tunnel profile is neutralized by the compressive in-situ stress. Thus, with an increase in the in-situ stress levels, the blast-induced damage gradually shrinks to a very thin zone near the tunnel contour. In deep tunnels under high in-situ stress conditions, the static component of dynamic stress redistribution becomes the main factor and dominates the development of EDZ. The transient unloading stress waves and blasting stress waves trigger or aggravate the damage extension. The PPV threshold for initiating blast damage first increases and then decreases as the in-situ stress level increases. Therefore, the effects of in-situ stress should be involved in the blasting vibration standards and damage criteria for underground blasting excavation.

Acknowledgments

This work is supported by Chinese National Natural Science Foundation (51509126 and 51409138), Jiangxi Provincial Natural Science Foundation (20161BAB206127), Scientific Research Key Fund of Jiangxi Provincial Department of Education (GJJ150030), and Opening Fund of State Key Laboratory of Water Resources and Hydropower Engineering Science (Wuhan University) (2015SGG01). The authors wish to express their thanks to all supports.

References

Adamson, W.R., Scherpenisse, C.R., 1998. The measurement and control of blast induced damage of final pit walls in open pit mining. In: Proceedings of the 24th Annual Conference on Explosives and Blasting Research, New Orleans, LA, pp. 539.
Blair, D.P., 2014. Blast vibration dependence on charge length, velocity of detonation and layered media. Int. J. Rock Mech. Min. Sci. 65, 29–39.
Cai, M., 2008. Influence of stress path on tunnel excavation response – numerical tool selection and modeling strategy. Tunn. Undergr. Space Technol. 23 (6), 618–628.
Cai, M., Kaiser, P.K., Tasaka, Y., Maejima, T., Morioka, H., Minami, M., 2004. Generalized crack initiation and crack damage stress thresholds of brittle rock masses near underground excavations. Int. J. Rock Mech. Min. Sci. 41 (5), 833–847.
Cao, W.Z., Li, X.B., Tao, M., Zhou, Z.L., 2016. Vibrations induced by high initial stress release during underground excavations. Tunn. Undergr. Space Technol. 53, 78–95.
Carter, J.P., Booker, J.R., 1990. Sudden excavation of a long circular tunnel in elastic ground. Int. J. Rock. Mech. Min. Sci. Geomech. Abstr. 27 (2), 129–132.
Cook, M.A., Cook, U.D., Clay, R.B., 1966. Behavior of rock during blasting. Trans. Soc. Min. Eng. 10 (2), 17–25.
Dare-Bryan, P.C., Mansfield, S., Schoeman, J., 2012. Blast optimisation through computer modelling of fragmentation, heave and damage. In: Proc. 10th Int. Symp. Rock Fragm. Blasting, New Delhi, India, pp. 95–104.
Fan, X., Wang, M.Y., Shi, C.C., 2009. Study on effects of initial stress on stress wave propagation and block movement law. Chinese J. Rock Mech. Eng. 28 (Supp. 2), 3442–3446 in Chinese, Abstract in English.
Fickett, W., Davis, W.C., 1979. Detonation. University of California Press, Berkeley, CA.
Hao, X.J., Feng, X.T., Yang, C.X., Jiang, Q., Li, S.J., 2016. Analysis of EDZ development of columnar jointed rock mass in the Baihetan diversion tunnel. Rock Mech. Rock Eng. 49 (4), 1289–1312.
He, M.C., Miao, J.L., Feng, J.L., 2010. Rock burst process of limestone and its acoustic emission characteristics under true-triaxial unloading conditions. Int. J. Rock Mech. Min. Sci. 47 (2), 286–298.
Henrych, J., Major, R., 1979. The Dynamics of Explosion and Its Use. Elsevier Scientific Pub. Co., Amsterdam and New York.
Holmberg, R., Persson, P.A., 1980. Design of tunnel perimeter blasthole patterns to prevent rock damage. Trans. Inst. Min. Metall., Sect. A 89, 37–40.
Jong, Y., Lee, C., Jeon, S., Cho, Y.D., Shim, D.S., 2005. Numerical modeling of the circular-cut using particle flaw code. In: 31st Annular Conference of Explosives and Blasting Technique, Orlando, CO., USA, CD-ROM.
Kaiser, P.K., Diederichs, M.S., Eberhardt, E., 2004. Damage initiation and propagation in hard rock during tunnelling and the influence of near-face stress rotation. Int. J. Rock Mech. Min. Sci. 41 (5), 785–812.
Krajcinovic, D., Silva, M.A.G., 1982. Statistical aspects of the continuous damage theory. Int. J. Solids Struct. 18 (7), 551–562.
Li, X.B., Gu, D.S., 1994. Rock Impact Dynamics. Central South University Press, Changsha (in Chinese).
Li, H.B., Xia, X., Li, J.C., Zhao, J., Liu, B., Liu, Y.Q., 2011. Rock damage control in bedrock blasting excavation for a nuclear power plant. Int. J. Rock Mech. Min. Sci. 48 (2), 210–218.
Li, S.J., Feng, X.T., Li, Z.H., Zhang, C.Q., Chen, B.R., 2012. Evolution of fractures in the excavation damaged zone of a deeply buried tunnel during TBM construction. Int. J. Rock Mech. Min. Sci. 55, 125–138.
Li, X.B., Cao, W.Z., Zhou, Z.L., Zou, Y., 2014. Influence of stress path on excavation unloading response. Tunn. Undergr. Space Technol. 42, 237–246.
Li, X., Zhang, Q.B., He, L., Zhao, J., 2017. Particle-based numerical manifold method to model dynamic fracture process in rock blasting. Int. J. Geomech. 17 (5), E4016014.
Lisjak, A., Tatone, B.S.A., Mahabadi, O.K., Grasselli, G., Marschall, P., Lanyon, G.W., de la Vaissiere, R., Shao, H., Leung, H., Nussbaum, C., 2016. Hybrid finite-discrete element simulation of the EDZ formation and mechanical sealing process around a micro-tunnel in Opalinus Clay. Rock Mech. Rock Eng. 49 (5), 1849–1873.
Lu, W.B., Yang, J.H., Yan, P., Chen, M., Zhou, C.B., Luo, Y., Jin, L., 2012. Dynamic response of rock mass induced by the transient release of in-situ stress. Int. J. Rock Mech. Min. Sci. 53 (9), 129–141.
Ma, G.W., An, X.M., 2008. Numerical simulation of blasting-induced rock fractures. Int. J. Rock Mech. Min. Sci. 45 (6), 966–975.
Martin, C.D., 1997. Seventeenth Canadian geotechnical colloquium: the effect of cohesion loss and stress path on brittle rock strength. Can. Geotech. J. 34 (5), 698–725.
Martino, J.B., Chandler, N.A., 2004. Excavation-induced damage studies at the underground research laboratory. Int. J. Rock Mech. Min. Sci. 41 (8), 1413–1426.
Omer, A., 2013. In situ stress inference from damage around blasted holes. Geosystem Eng 16 (1), 83–91.
Persson, P.A., Holmberg, R., Lee, J., 1993. Rock Blasting and Explosives Engineering. CRC Press, Boca Raton.
Ramulu, M., Chakraborty, A.K., Sitharam, T.G., 2009. Damage assessment of basaltic rock

mass due to repeated blasting in a railway tunnelling project – a case study. Tunn. Undergr. Space Technol. 24 (2), 208–221.
Read, R.S., 2004. 20 years of excavation response studies at AECL's Underground Research Laboratory. Int. J. Rock Mech. Min. Sci. 41 (8), 1251–1275.
Siren, T., Kantia, P., Rinne, M., 2015. Considerations and observations of stress-induced and construction-induced excavation damage zone in crystalline rock. Int. J. Rock Mech. Min. Sci. 73, 165–174.
Stagg, M.S., Siskind, D.E., Stevens, M.G., Dowding, C.H., 1984. Effects of repeated blasting on a wood-frame house. BuMines RI 8896, 81–82.
Starfield, A.M., Pugliese, J.M., 1968. Compression waves generated in rock by cylindrical explosive charges: a comparison between a computer model and field measurements. Int. J. Rock Mech. Min. Sci. 5 (1), 65–77.
Torano, J., Rodríguez, R., Diego, I., Rivas, J.M., Casal, M.D., 2006. FEM models including randomness and its application to the blasting vibrations prediction. Comput. Geotech. 33 (1), 15–28.
Wei, W., Jiang, Q.H., Peng, J., 2017. New rock bolt model and numerical implementation in numerical manifold method. Int. J. Geomech. 17 (5), E4016004.
Xia, X., Li, H.B., Li, J.C., Liu, B., Yu, C., 2013. A case study on rock damage prediction and control method for underground tunnels subjected to adjacent excavation blasting. Tunn. Undergr. Space Technol. 35, 1–7.
Xie, L.X., Lu, W.B., Zhang, Q.B., Jiang, Q.H., Wang, G.H., Zhao, J., 2016. Damage evolution mechanisms of rock in deep tunnels induced by cut blasting. Tunn. Undergr. Space Technol. 58, 257–270.
Yan, P., Lu, W.B., Chen, M., Hu, Y.G., Zhou, C.B., Wu, X.X., 2015. Contributions of in-situ stress transient redistribution to blasting excavation damage zone of deep tunnels. Rock Mech. Rock Eng. 48 (2), 715–726.
Yang, J.H., Lu, W.B., Hu, Y.G., Chen, M., Yan, P., 2015. Numerical simulation of rock mass damage evolution during deep-buried tunnel excavation by drill and blast. Rock Mech. Rock Eng. 48 (5), 2045–2059.
Yang, J.H., Lu, W.B., Jiang, Q.H., Yao, C., Jiang, S.H., Tian, L., 2016a. A study on the vibration frequency of blasting excavation in highly-stressed rock masses. Rock Mech. Rock Eng. 49 (7), 2825–2843.
Yang, J.H., Lu, W.B., Yan, P., Yao, C., Zhou, C.B., Wang, Z.L., 2016b. Prevention method for rock bursts based on control of dynamic effects caused by transient release of in situ stresses. Chin. J. Geotech. Eng. 38 (1), 68–75 in Chinese, Abstract in English.
Yao, C., Shao, J.F., Jiang, Q.H., Zhou, C.B., 2017. Numerical study of excavation induced fractures using an extended rigid block spring method. Comput. Geotech. 85, 368–383.
Yilmaz, O., Unlu, T., 2013. Three dimensional numerical rock damage analysis under blasting load. Tunn. Undergr. Space Technol. 38, 266–278.
Zhang, C.Q., Feng, X.T., Zhou, H., Zhang, C.S., Wu, S.Y., 2010. Brittle failure of surrounding rock mass in deep test tunnels and its numerical simulation. Chinese J. Rock Mech. Eng. 29 (10), 2063–2068 in Chinese, Abstract in English.
Zhang, Q.B., Zhao, J., 2014. A review of dynamic experimental techniques and mechanical behaviour of rock materials. Rock Mech. Rock Eng. 47 (4), 1411–1478.
Zhu, W.C., Wei, J., Zhao, J., Niu, L.L., 2014. 2D numerical simulation on excavation damaged zone induced by dynamic stress redistribution. Tunn. Undergr. Space Technol. 43, 315–326.
Zhu, Z., Mohanty, B., Xie, H., 2007. Numerical investigation of blasting-induced crack initiation and propagation in rocks. Int. J. Rock Mech. Min. Sci. 44 (3), 412–424.